Journal of Geophysical Research: Solid Earth

Supporting Information for

The lithospheric structure of the Gibraltar Arc System from Wide Angle Seismic data

Laura Gómez de la Peña[1], Ingo Grevemeyer[1], Heidrun Kopp[1,2], Jordi Díaz[3], Josep Gallart[3], Guillermo Booth-Rea[4], Eulàlia Gràcia[5] and César R. Ranero[5,6]

[1]GEOMAR Helmholtz Centre for Ocean Research Kiel, Germany

[2]Christian-Albrechts-Universität zu Kiel, Kiel, Germany

[3]Institute of Earth Sciences Jaume Almera, CSIC, Barcelona, Spain

[4]Instituto Andaluz de Ciencias de la Tierra UGR-CSIC, Granada, Spain

[5]Barcelona Center for Subsurface Imaging, Institut de Ciències del Mar, CSIC, Barcelona, Spain

[6]ICREA, Passeig de Lluis Companys 23, 08010, Barcelona, Spain

Contents of this file

Introduction

Description of the steps followed during the WAS data inversion, the model parameters and the misfit between the observed and calculated travel times.

Text S1. Joint refraction and reflection tomography

In order to obtain the Vp wave velocity model, we used the tomo2D software (Korenaga et al., 2000) to perform the joint inversion of refracted and reflected phases. The initial velocity model is a 1D-velocity model extrapolated along the entire profile and hanging from the topography/bathymetry (Fig. S1a). This 1D velocity model is obtained from inversion of P- and S-wave arrivals of local earthquakes (Grevemeyer et al., 2015). For the initial model definition, we constrained the sedimentary layer geometry and velocity from the Ps refractions and the PsP reflections, and defined a velocity gradient for the crust fixing the velocity at three different depths: 4.2 km/s below the basement top, 6.2 km/s at 3.5 km depth below the basement top and 6.8 km/s at 20 km depth below the basement top (Fig. S1a). The node spacing of the velocity grid is 1 km along the profile and 0.25 km in depth.

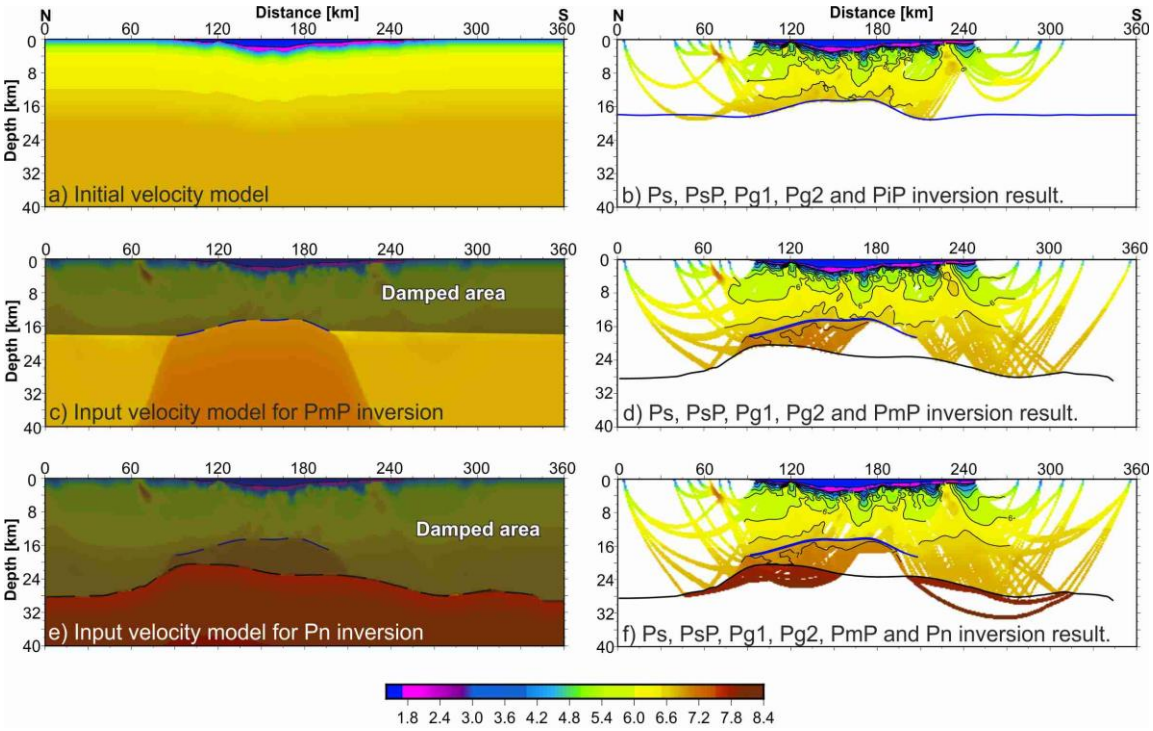

Figure S1. *Initial velocity model and input velocity models for consecutive steps in the inversion. a) Initial velocity model for the inversion. b) Inverted model using phases Ps, PsP, Pg1, Pg2 and PiP, masked by the ray paths. c) Input velocity model for the PmP inversion, which is the velocity model resulting of the inversion of the Ps, PsP, Pg1, Pg2 and PiP phases, damped and modified to include a high velocity lower crust. d) Inverted model using phases Ps, PsP, Pg1, Pg2 and PmP, masked by the ray paths. e) Input velocity model for the Pn inversion, which is the velocity model resulting of the inversion of the Ps, PsP, Pg1, Pg2 and PmP phases, damped and modified to include mantle velocities below the inverted Moho reflection. f) Inverted model using Ps, PsP, Pg1, Pg2, PmP and Pn phases, masked by the ray paths.*

To perform the inversion, we followed a layer-stripping strategy. We started the inversion with the shallower phase. Then, we updated the initial velocity model with the results of the inversion of this phase and used the updated model as input velocity model for the next inversion (Fig. S1). Only one reflected phase can be inverted at a time, so we first inverted the sediment thickness (Fig. S1a), then the PiP location (Fig. S1b) and finally the PmP location (Fig. S1d). In order to maintain the geometry of the PiP reflection and the velocity structure above it, we damped this area of the profile prior to the PmP inversion (Fig. S1a-d). A relatively high-velocity anomaly is needed in the starting model to fit the arrivals running through the lower crust (Fig. S1c). Finally, we applied damping to the entire crust before inverting the Pn (Fig. S1e, f). The initial velocity for the mantle has been also approximated from the 1D velocity model presented in Grevemeyer et al. (2015), ranging between 7.7 and 8.25 km/s (Fig. S1e).

To obtain the geometry of the reflections, two initial reflections are used. For the PiP reflection, the initial reflection is a horizontal reflection at 18 km depth. For the PmP, we used a reflection located at 30 km depth below the onshore stations and at 25 km depth offshore. We gave an equal weight to the picked reflections and refractions. The smoothing is defined in vertical and horizontal directions, and increases with depth (Table S1).

We have followed the same criteria for phase identification as in profile p02 (Booth-Rea et al., 2018). The correlation lengths at top and bottom of the two profiles are similar (Table S1), and small differences are driven by the different station spacing along both profiles and the number of arrivals from the PmP reflection.

	p01	p02
Horizontal correlation length - top	2	2
Horizontal correlation length - bottom	6	6
Vertical correlation length - top	1	2
Vertical correlation length - bottom	5	5
PiP correlation length	3	3
PmP correlation length	5	3

Table S1. *Correlation lengths (smoothing parameters) applied to the p01 and p02 velocity models.*

- **Observed travel time vs. calculated travel time**

We used the misfit between the observed travel times and the calculated travel times to assess the accuracy of our results. The misfit between the observed and the calculated travel times for the different phases inverted is displayed in Table S2. Examples of plotted record sections together with the observed and calculated travel times are shown in Figure 2 of the main manuscript.

Phase	Root Mean Square misfit (s)	chi-squared value, χ^2
Ps	0.0330	0.6812
Ps + Pg1	0.0382	0.6192
Ps + Pg1+Pg2	0.0609	1.1284
Ps + Pg1+Pg2+PiP	0.1009	1.2706
Ps + Pg1+Pg2+PmP	0.0933	1.8142
Ps + Pg1+Pg2+PmP+Pn	0.1010	1.8582

Table S2. *Misfit between the observed and the calculated travel times for the phases inverted.*

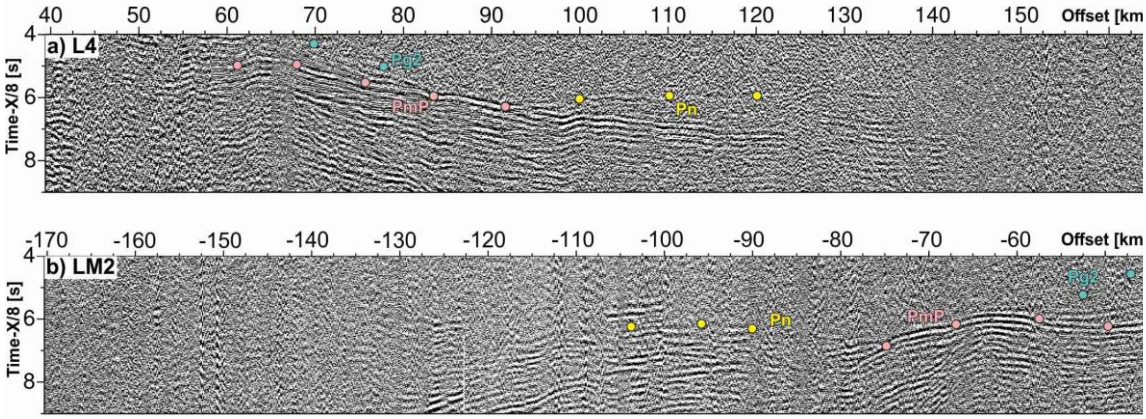

Figure S2. *Record section of land stations L4 (a) and LM2 (b) reduced by 8 km/s. Phase Pn, travelling at a velocity ~8 km/s, is colored in yellow. The same two sections reduced by 6 km/s are shown in Figure 2a and 2e of the main manuscript.*

References:

Booth-Rea, G., R. Ranero, C., & Grevemeyer, I. (2018). The Alboran volcanic-arc modulated the Messinian faunal exchange and salinity crisis. *Scientific Reports,* 8(1), 1–14. https://doi.org/10.1038/s41598-018-31307-7

Grevemeyer, I., Gràcia, E., Villaseñor, A., Leuchters, W., & Watts, A. B. (2015). Seismicity and active tectonics in the Alboran Sea, Western Mediterranean: Constraints from an offshore-onshore seismological network and swath bathymetry data. *Journal of Geophysical Research: Solid Earth*, 120, 767–787. https://doi.org/10.1002/2015JB012352.

Korenaga, J., Holbroook, W.S., Kent, G.M., Kelemen, P.B., Detrick, R.S., Larsen, H.C., Hopper, J.R. & Dahl-Jensen, T. (2000). Crustal structure of the southeast Greenland margin from joint refraction and reflection seismic tomography. *Journal of Geophysical Research*, 105(B9), 21591–21614.